

Article

Validation of a New Method for Continuous Flare Combustion Efficiency Monitoring

Chong Tao ^{1,*}, Jon Chow ¹, Lei Sui ¹, Anan Wang ¹, Gerard Bottino ¹, Peter Evans ², David Newman ², Raj Venuturumilli ², Jon Lowe ² and Johan Liekens ²

¹ Baker Hughes, 1100 Technology Park Dr, Billerica, MA 01821, USA; jon.chow@bakerhughes.com (J.C.); lei.sui@bakerhughes.com (L.S.); anan.wang@bakerhughes.com (A.W.); gerard.bottino@bakerhughes.com (G.B.)

² bp, Sunbury on Thames, London TW16 7LN, UK; peter.evans@uk.bp.com (P.E.); david.newman@uk.bp.com (D.N.); raj.v@bp.com (R.V.); jon.lowe@bp.com (J.L.); johan.lieken@ec1.bp.com (J.L.)

* Correspondence: chong.tao@bakerhughes.com

Abstract: A new method is described for calculating flare combustion efficiency (CE) and destruction and removal efficiency (DRE) using a numerical parametric model. The method combines key variables that affect flare performance including the flare vent gas net heating value (NHV), flare design, flow rate, exit velocity, and inert gas composition, alongside the environmental influence of crosswind speed. Each effect is characterized using a parametric model derived from experimental testing data and computational fluid dynamics (CFD). The inclusion of CFD allows the model to be extended into the high-wind conditions that cannot be adequately controlled for in empirical testing yet represent some of the most challenging conditions in which to maintain good combustion. This new parametric model method (PMM) is coupled with ultrasonic flowmeters from which the molecular weight and net heating value of the flare gas can be derived using the vent gas speed of sound measurement. In doing so, this method provides a reliable continuous flare combustion efficiency measure that can be deployed at scale with minimum hardware updates. The system was verified using an extractive sampling method with tests conducted on three full-scale industrial flares including non-assisted, single-arm pressure-assisted, and multi-arm pressure-assisted flare designs. A total of seventy valid test points were carried out with varying flow rate and flare gas heating value, covering a CE range from 46–100%. The uncertainty of the method was assessed using both traditional error propagation and Monte Carlo methodology. The results from the new method agree with the extractive method to within 0.8% in the $\geq 98\%$ DRE region where flares are expected to operate to limit the impacts of flaring as a source of methane as a greenhouse gas. Uncertainty analysis revealed that the larger DRE discrepancy for $DRE \leq 98\%$ correlates to the measurement uncertainties for both methods.

Keywords: flare; combustion efficiency monitoring; flare combustion efficiency



Citation: Tao, C.; Chow, J.; Sui, L.; Wang, A.; Bottino, G.; Evans, P.; Newman, D.; Venuturumilli, R.; Lowe, J.; Liekens, J. Validation of a New Method for Continuous Flare Combustion Efficiency Monitoring. *Atmosphere* **2024**, *15*, 356. <https://doi.org/10.3390/atmos15030356>

Academic Editor: Wei-Ping Hu

Received: 23 February 2024

Revised: 9 March 2024

Accepted: 12 March 2024

Published: 14 March 2024



Copyright: © 2024 by the authors. Licensee MDPI, Basel, Switzerland. This article is an open access article distributed under the terms and conditions of the Creative Commons Attribution (CC BY) license (<https://creativecommons.org/licenses/by/4.0/>).

1. Introduction

Flares are open combustion devices for emergency pressure relief and for burning off waste and unwanted gas. They can be found in both upstream and downstream sectors of the oil and gas industry. Whilst significant improvements have been made to reduce routine flaring, the development of alternate technologies that can prospectively replace flares is limited. Therefore, their role as a critical safety device will persist well into the energy transition era.

Recently, the role of flaring as a source of greenhouse gases has come under increased scrutiny because of their potential to be a significant source of methane. Methane is the principal component of natural gas but has a global warming potential 28 times greater than that of CO₂ over a 100-year period. The effect is also more than 84 times higher over

a 20-year period according to the Intergovernmental Panel on Climate Change (IPCC) Assessment Report 5. Reducing methane emissions has therefore become a key action in tackling temperature rises. The World Bank flare tracker estimates over 150 billion cubic meters (bcm) of gas is flared annually, with 90% coming from the upstream sector [1].

Combustion efficiency (CE) is one of the key parameters for effective flare operation. It is a measure of the percentage of hydrocarbons that undergo complete combustion and are converted into CO₂ and H₂O. For environmental reporting, this is normally extended to include incomplete combustion products such as CO and soot and referred to as the destruction and removal efficiency (DRE). The convention is to estimate that 98% of the combustible gases burn—releasing 2% to the atmosphere. However, recent studies, such as that by Plant et al., show that the estimated flare efficiency is much more varied [2]. Even after the effect of unlit flares has been accounted for, efficiency still varies from <90% to over 99%.

In 2023, the US government published the “Greenhouse gas reporting rule for petroleum and natural gas systems” through the Environmental Protection Agency (EPA) [3]. In the proposed rule, the flare combustion efficiency used for flare emissions reporting calculations will be divided into three tiers depending on the level of conformity of flare monitoring system requirements, instead of a single fixed value of 98%. A flare combustion efficiency of 98% can be applied to flare emission calculations for tier 1, with a CE of 95% and CE of 92% for tier 2 and tier 3, respectively. When evaluating the environmental impact of upstream flaring, accurate flaring efficiency rather than using an estimated fixed value is critical.

Flare CE/DRE has been the subject of both experimental and theoretical studies. Since the first comprehensive flare combustion efficiency study by the US EPA in 1983 [4], an extractive sampling method, where samples of the flare plume were extracted after flare combustion and the products assayed for CE and DRE, has become the de facto standard method for industrial flare CE measurement. This was the principal method behind one of the most extensive experimental studies for refinery flares directed by the Texas Commission for Environmental Quality (TCEQ) and carried out by the University of Texas Austin in 2010 [5]. This study generated extensive results for assisted flares (steam-assisted and air-assisted flares often used in refineries and petrochemical plants) in helping flare operators to optimize flare operations as well as helping regulatory bodies in policy making for flare operations, but less data were obtained for flares without assist gases, which constitute the majority of upstream flares.

The extractive sampling method is considered as the most accurate benchmark method in CE/DRE measurement as it directly measures the flare plume gas. However, due to its instrumentation and data analysis complexity and manual process of sample extraction, only a couple of flare testing facilities exist worldwide, and these are only suited for research and impractical to be employed for CE measurement in the field.

To overcome the practical limitations of full-scale testing and exploration of the effects of wind speed, Johnson and colleagues measured the crosswind effect, using wind up to 17 m/s, on lab-scale flares fueled by natural gas, ethane, and propane in a wind tunnel [6]. A limitation of this work is that scaled-down flares lack many of the more advanced design and geometries that are commonplace in the field that have been implemented to enhance combustion.

Recently, computational fluid dynamics (CFD) with different combustion models, such as eddy dispersion concept (EDC) and probability density function (PDF), coupled with an even more complete reaction mechanism, have been used to understand flare combustion. Factors affecting flare combustion efficiency have also been studied by several research groups, including studies by Edgar [7], Chen [8], and Black [9]. CFD has been a complimentary tool, especially to test out conditions that cannot be controlled or achieved in testing facilities. The lowering of computational cost and increase in cloud-based high-performance computing (HPC) capability have made accurate combustion efficiency

calculation for industrial-scale flares possible, especially with the progress of reaction kinetic models in CFD.

Monitoring and measuring industrial flare combustion efficiency in the field has been a longstanding challenge. This is because industrial flares are open combustion, large in scale, and subject to large variations in operation conditions. Technologies such as differential absorption lidar (DIAL) and passive Fourier transform spectrometry (pFTIR) have been used to test flares [10,11]. DIAL uses an active laser source, whereas pFTIR uses the thermal radiation of combustion. For both methods, gas species' mass emission rate from a source can be calculated using the measured hydrocarbon concentration map and wind speed. Coupled with the total flare gas flowrate, flare DRE can be calculated. In general, they have only been used for research or for spot checks of flare efficiency. They are unsuitable for continuous flare efficiency monitoring due to system complexity and lack of automation.

One of the more practical approaches to measure flare CE is to use remote monitoring technique such as hyperspectral infrared imager. It measures unburned hydrocarbons and CO₂ concentration in the combustion plume in the mid-infrared spectrum region (as demonstrated by Zeng et al. [12]). It has shown high accuracy in flare CE measurement compared to the extractive sampling method, with an average error of 0.5% for the test cases published in the paper. This type of instrument can be made relatively compact and field-deployable. However, harsh environment and adverse weather conditions, such as wind and heavy fog/rain pose challenges for the camera technology. Flares with small flame size or low-heating-value vent gas will cause errors for this optical method, which has limited camera pixel size.

In response to these existing limitations, a new flare CE/DRE measurement and monitoring method has been developed by Tao using a parametric modeling method (PMM) [13]. This method uses artificial intelligence (AI) to analyze the available CE measurement data and computational fluid dynamics (CFD) data to generalize all the factors affecting combustion efficiency (CE) in a flare system. The factors include crosswind speed and process conditions, such as flare flow rate, vent gas exit velocity, flare tip diameter, vent gas molecular weight, vent gas NHV, and gas composition. For assisted flares, assisted gas (steam or air) flow rate and NHV in the combustion zone (NHV_{cz}) are considered. The smoke formation model is also included in the method. Each factor has a different weighting on the effect on CE, as well as cross terms involving multiple factors. These effects are generalized into a numerical model to calculate the CE. Destruction and removal efficiency (DRE) can then be derived from the calculated CE as they have shown a near-linear relationship. Three different CE models were developed for steam-assisted, air-assisted, and non-assisted (including pressure-assisted) flares.

On a system level, one of the key features of this flare combustion efficiency monitoring system is that it can be built upon an ultrasonic flare flowmeter. Specifically, ultrasonic flare flowmeters are designed to measure flowrate based on ultrasound transit "time of flight" across the flow, where the flow and ultrasonic beam intercept at a fixed angle. And because sound waves travel faster along the flow and slower against the flow, the time difference is the transit time. Flare gas flowrate can be measured from this transit time. In addition, from the vent gas speed of sound (SOS), the average molecular weight (MW) can be derived using the virial equation of state for sound speed as shown by Hammond [14]. From the average MW and concentrations of noncombustible gases (such as N₂, CO₂, etc.), flare gas net heating value can be determined as shown in the patent [15]. Therefore, with the measurement of flare gas flowrate, and NHV and MW from the ultrasound flowmeter, key parameters affecting flare combustion efficiency are available. Moreover, using the wind speed measurement, a complete flare combustion efficiency monitoring system—including the flowmeter and an industrial computer loaded with the model—can provide real-time measurement and continuous monitoring of flare CE/DRE.

In this paper, an experiment was conducted with sample extraction method on full-scale flares to verify the new PMM-based flare combustion efficiency method, specifically for upstream applications where natural gas is the dominating fuel gas. A simple flare

efficiency measurement and monitoring system can be built on the PMM method with an ultrasonic flowmeter. Key information for flare operation, such as flare gas MW and NHV, can be derived from gas speed of sound provided by the flowmeter. This enables the whole flare efficiency measurement/monitoring system to be easily deployable and scalable.

2. Methods

A test regime was designed to evaluate the PMM method under various controllable flare process conditions and flare designs. A brief description of the experimental setup will be provided in this section with further details in a second paper [16]. All tests were conducted at the John Zink (JZ) test facility in Tulsa Oklahoma in January–February 2023. This facility has previously been used for related studies, including the TCEQ flare study in 2010. Considering the availability of flare tips, and using flare tip designs reflecting flare types commonly used in upstream applications, testing was conducted using three tips, as shown in Figure 1. These include a 14" non-assisted straight pipe flare tip with an effective flare tip diameter of 11" (utility flare), a single-arm pressure-assisted 8" flare with an effective diameter of 5.2" (sonic), and an 8" multi-arm pressure-assisted sonic flare with an effective tip diameter of 5.26" (hydra). Sonic and hydra flares have the same exit area, allowing the impact of flare geometry to be tested.



Figure 1. Three flare tips used for the experiment: (a) sonic—with restricted orifice shown; (b) pressure-assisted multi-arm ‘hydra’ flare tip, and (c) single-pipe non-assisted ‘utility’ flare tip.

The test involves the measurement of CE/DRE for a given test condition using the JZ sample extraction method and PMM prediction method. As illustrated in Figure 2, nitrogen and grid-supplied gas were metered separately using orifice plate flowmeters with $\frac{1}{2}$ " to 4" diameter orifice depending on flowrate and then mixed. As part of the parametric model flare CE monitoring system, a 6-inch ultrasonic flowmeter (Panametrics model GF) coupled with pressure (P) and temperature (T) probes and transmitters was installed downstream of the gas mixing panel. The outputs from the flowmeter, including volumetric flowrate and flare gas speed of sound, were fed to the JZ flare-testing distributed control system (DCS). To measure the vent gas composition, a sample of flare gas was drawn to a Fourier transform infrared spectrometer (FTIR) gas analyzer. The vent gas mixture was flowing in a 14" diameter pipe adaptor connecting the pipe and flare stack. For both the 8" sonic and hydra flare tips, a pipe reducing adaptor spool was used. A 2" flare pilot burning Tulsa natural gas (TNG) was used to ignite the flare and keep it lit for low-NHV gas. The flue gas right after the combustion was extracted by a gas extraction probe held with a crane. The exact probe position and orientation were manually adjusted. Three thermocouples are located around the edge of the gas sampler to measure the temperature of the flue gas drawn in. The temperature was recorded to validate the test points, showing it was between 400° F and 700° F. This was used to ensure that was the plume was captured. The extracted flue gas was then sent to the flue gas analyzers to measure the concentration of

CO, NO_x, CO₂, O₂, and unburnt hydrocarbons (HC). All the gas analyzers and FTIR were carried by the JZ Air Source Mobile Lab, equipped with wireless data transfer capability to send the measurement data over to the DAQ system. A weather station located in an open field about 400 feet away from the test spot measuring barometric pressure, ambient temperature, relative humidity, and wind speed was connected to the DAQ system using wireless communication. The test methods and procedures used were consistent with standard EPA methods for stack testing.

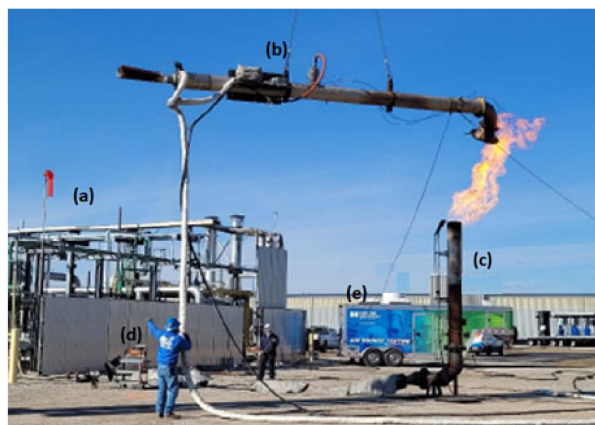


Figure 2. Experimental setup includes: (a) gas panel; (b) sample extraction probe; (c) flare stack; (d) ultrasonic flowmeter; and (e) gas analyzer mobile laboratory.

As in field applications, the standalone flare control or flare combustion efficiency monitoring is connected to the site DCS to ensure data integrity and fast time response. A standalone flare combustion efficiency monitoring system with the parametric model installed was connected to the DCS system, where the inputs/outputs were transferred via Modbus TCP/IP communication. The required inputs for the new method include flare flowrate, vent gas pressure (P) and temperature (T), speed of sound, N₂ concentration, flare tip diameter, and wind speed. Specifically, from flare gas speed of sound and P/T, the average MW can be calculated. The NHV of flare gas can also be derived from the average MW and N₂ concentration. With the inputs for this flare CE monitoring system, it outputs the calculated CE and DRE, which were compared to the measured CE/DRE using sample extraction method. Each test data point required 5 min of testing for a valid measurement of CE for sample extraction method and was repeated three times consecutively (effectively 15 min continuous testing for each measurement point), whilst monitoring the extraction thermocouples to ensure sampling remained within the plume. If the temperature dropped, the test period was extended. Quality assurance of the CE/DRE measurement included the oxygen level of the extracted sample, hydrocarbon mass balance, and N₂ concentration validation between flowrate and FTIR. Input and output data were transferred between the DCS and parametric model system at a 1 Hz rate. Averaged CE/DRE results from both the sample extraction method and parametric model were used for the analysis. Due to the update limitation of ultrasonic flowmeter, the actual time for CE/DRE measurement of the system is 2 s. The measured CE/DRE values were averaged over the 5 min period for each test point. The final CE/DRE value presented in this paper is the averaged results from the three consecutive measurements.

Flare CE and DRE in the testing are defined as follows:

$$CE(\%) = \frac{[CO_2]}{[CO_2] + [CO] + [THC]} \times 100 \quad (1)$$

where CE(%) is the flare combustion efficiency in percentage; [CO₂], [CO], and [THC] are dry gas concentrations of CO₂, CO, and total hydrocarbons as dry CH₄, respectively. Dry gas concentrations of CO₂ and CO of the sampled flue gas were directly measured by the

gas analyzers in the mobile lab. The total hydrocarbon concentration was measured on a wet basis and was converted to dry basis by accounting for moisture content in the flue gas.

$$\text{DRE}(\%) = \left(1 - \frac{\text{THC}_{\text{out}}}{\text{THC}_{\text{in}}}\right) \times 100 \quad (2)$$

where DRE(%) is the flare destruction and removal efficiency in percentage; THC_{out} is the exhaust of total hydrocarbon in Lbs/h from the flare stack emission; and THC_{in} is the total hydrocarbon flow rate in Lbs/h before the combustion. The exhaust of total hydrocarbon, THC_{out} , can be calculated based on the tracer gas of CO_2 using standard US EPA method 19 [17].

The DRE used in the parametric model is defined the same as in the extractive sampling method. The CE in the parametric model includes the soot formation model, and is defined as:

$$\text{CE}(\%) = \frac{[\text{CO}_2]}{[\text{CO}_2] + [\text{CO}] + [\text{THC}] + [\text{soot}]} \times 100 \quad (3)$$

where [soot] is the soot concentration measured as carbon particle concentration. For all the validation tests in the paper, no visible emission was observed, and soot formation was negligible. Therefore, the CE and DRE of both the JZ test and parametric model can be compared directly.

The experimental design included the use of an independent flare pilot. The pilot was designed with a fixed fuel supply of TNG (Tulsa natural gas) of the same origin and composition as that used in the main flare. It has a constant flow of 87 SCFH (standard cubic feet per hour) and was designed to operate with an effective CE/DRE of 100%. The experimental protocol includes consideration of the role of the pilot in deriving CE/DRE under a range of conditions.

It is important to include measurement uncertainty to show measurement accuracy and quality. Uncertainty of the measurements was estimated in accordance with the Guide to Expression of Uncertainty in Measurement, often referred to as the GUM (ISO/IEC Guide 98-3:2008) [18]. The empirical testing (JZ) results are reported with an estimate of uncertainty by the vendor using the error propagation method. For test cases with large uncertainties, quality of the measurement may need improvement to obtain definitive values.

The test matrix includes three different exit velocities (covering low, medium, and high flare flowrate conditions), three different NHV conditions (low, medium, and high heating values with adjustment of dilution ratio of TNG gas with N_2), and the three above-mentioned flare tip designs. The test conditions of all 70 valid test cases are summarized in Table A1 in Appendix A. The flares were operated by JZ personnel, and the test conditions in Table A1 were proved by JZ from their central data acquisition (DAQ) system. As described earlier, the main purpose of the testing is to validate the parametric model over flare conditions of NHV (high, medium, and low NHV of 900, 600, and 300 BTU/SCF, respectively) and flow exit velocity (high, medium, and low velocities of 5, 0.6, and 0.2 m/s) for the three different flare types.

In addition to the 27 designed test cases, extra testing points—mainly in the low heating value regions of $\text{NHV} < 300$ BTU/SCF—were carried out to understand flare combustion behavior in this CE transitional region, as well as to test the model in the extremely low NHV region. For the test cases where the flare could not maintain a stable combustion, up to three duplicate tests were conducted to obtain reliable measurements and check test repeatability. The repeatability is consistent with the overall uncertainty, as discussed in the following section. For the region of $\text{NHV} < 300$ BTU/SCF, the typical repeatability is within 3.3% (absolute).

3. Results

All results are summarized in Table A2 in Appendix A. The results include measured CE and DRE with associated uncertainties for the 70 test points. CE and DRE results from the PMM method and associated uncertainties generated from direct error propagation

method and Monte Carlo method (MCM). The measurement uncertainties for both the extractive sampling method and new PMM method are listed and will be discussed later in this session.

Both CE and DRE are effective parameters for flare efficiency measurement and have strong correlation, especially in the high-efficiency region where flare was designed to operate. The overall results for both CE and DRE are tracking each other as DRE is derived from CE using linear interpolation in PMM. In addition, it is often more convenient to use DRE to calculate unburnt hydrocarbons from total vent gas flowrate for flare emissions calculation as adopted in most regulations. For simplicity, DRE will be used in the discussion below.

3.1. Verification Results

Figure 3 shows the comparison of DRE% from JZ extractive sampling measurement and PMM calculation, with associated measurement uncertainties derived using the error propagation method. They are plotted against the vent gas net heating value (NHV). DRE goes through a sharp transition from NHV of 160 BTU/SCF to NHV of 300 BTU/SCF and plateaus beyond that, as shown by both measurements. The DRE varies dramatically from 46% to 98% in this transition region and reaches close to 100% in the plateau with much smaller measurement uncertainties. The DRE values from the PMM method match those of the experimentally measured DRE when $\text{NHV} > 300$ BTU/SCF with average difference of 0.83% (absolute value), as shown in Figure 4. The two points, test case 26 and 27 had larger measurement errors in the $\text{NHV} > 600$ BTU/SCF region, which was associated with small flowrates and larger variations for the JZ test. Considering the DRE uncertainties and difference of both methods, the PPM method provides accurate measurement of DRE in the region.

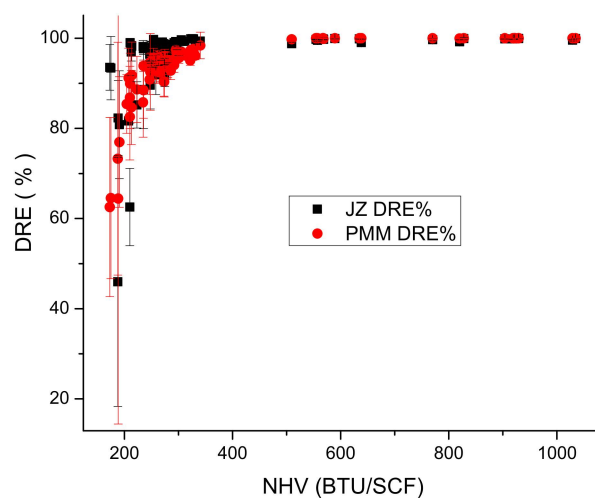


Figure 3. Comparison of DRE from the new modeling method, PMM method (red), and John Zink (JZ) experiment measurement (black) with associated uncertainties (1σ) from error propagation method.

As the NHV value drops below 300 BTU/SCF, DRE values start to decrease and show large variations for different test conditions such as flow rate and crosswind speed, especially for the regions where $\text{NHV} < 250$ BTU/SCF. In these NHV regions, flare flame was unstable for most of the test points requiring the need for a continuous pilot. This result aligns with US EPA Refinery Sector Rules that stipulate that NHV in the combustion zone (NHV_{cz}) should be maintained above 270 BTU/SCF [19]. Comparing the DRE results of the JZ test and PMM measurement, the average DRE% differences are 3.63% and 10.59% for regions of $250 < \text{NHV} < 300$ BTU/SCF and $\text{NHV} < 250$ BTU/SCF, respectively. These large discrepancies are correlated with the larger measurement uncertainties for both methods as discussed in the following section.

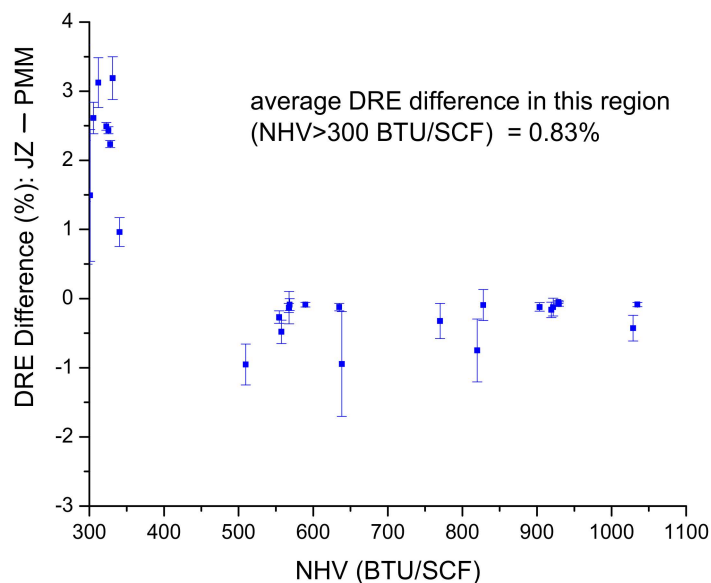


Figure 4. DRE difference between JZ measured value and PMM value for NHV > 300 BTU/SCF with associated uncertainty error bar for JZ test.

3.2. Uncertainty Analysis of JZ Test and PMM Measurement

The JZ CE/DRE measurement uncertainties were mainly introduced by instrument errors and testing variabilities, such as sample extraction variation. Specifically, based on measurement uncertainties of all the inputs, such as CO₂, CO, flare gas composition measurement, and so on, and their sensitivity coefficients, the CE/DRE error caused by instruments can be derived. The uncertainty caused by gas sampling can be estimated from the repeatability of CE/DRE measurement. The overall system level of CE/DRE uncertainty can be derived as the root sum square of the instrument error and sample extraction error. The detailed CE/DRE uncertainty calculation for the JZ measurement can be found in the accompanying paper [16]. The uncertainty of the PMM method has been assessed using two independent methodologies that conform to the GUM. In the first method, the error was propagated in the same way as that used by the JZ tests. In the second method, to provide a semi-independent assessment of the uncertainty, the data were analyzed using Monte Carlo method (ISO/IEC GUIDE 98-3/Suppl.1, 2008) [20], in which each input is assigned a probability density function (PDF) and then randomly tested over 1 million trials to derive a coverage probability of 95%. The mean value within the coverage was selected as the expected value. The distance between the mean value and the coverage range was deemed to be the corresponding uncertainty. The Python platform was employed to implement the PMM calculation and MCM analysis. Figure 5 highlights the corresponding information of the MCM analysis for test point 7, including the distribution of the inputs and outputs.

Validation of the MCM process was performed according to the ISO guide for each test case. The validation checklist includes: the model is continuous with respect to the generated values from PDF of each input; the distribution function for the output value is continuous and strictly increasing; PDF for the output is continuous and unimodal (single-peaked) and monotonic to the left or right of the mode; expectation from the outcome and its variance exist; and large enough trials (M) were used. For the 70 cases analyzed by the method, all the results were checked and passed the validation.

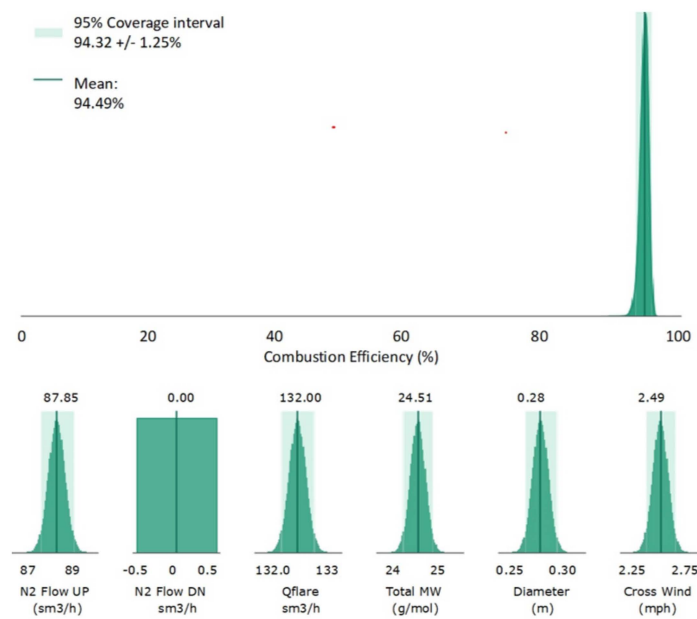


Figure 5. Example of MCM determination of parametric model CE/DRE uncertainty.

Figure 6 shows the uncertainties of DRE for PMM measurement with two standard deviations (2σ), or 95% confidence level from both direct error propagation and MCM methods. Note that the uncertainties are plotted in positive values for clear comparison, instead of $+/-$ range. The uncertainties from both methods are consistent with each other (shown in the main plot), except for five extreme cases where the direct error propagation method did not have any limit for the DRE calculation (shown in the insert), as it should be capped to a value of 0–100%. The average uncertainty from the MCM method for the $NHV > 300$ BTU/SCF region, where DRE is at $>98\%$, is $\pm 0.37\%$ (2σ). For regions below 300 BTU/SCF, the PMM uncertainties calculated from the MCM method increase with the values of $\pm 3.50\%$ and $\pm 14.67\%$ for regions of $250 < NHV < 300$ BTU/SCF and $170 < NHV < 250$ BTU/SCF, respectively.

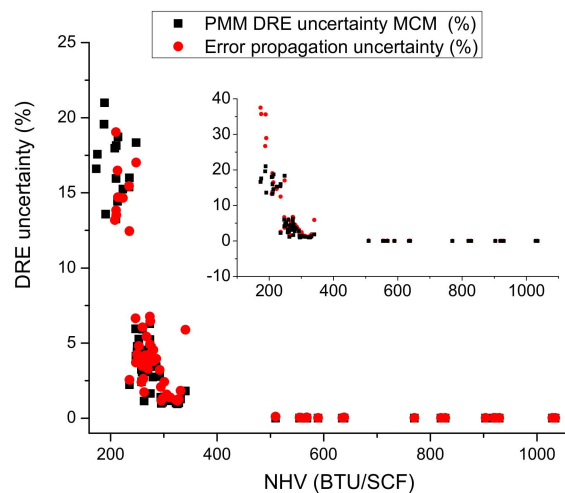


Figure 6. PMM uncertainties calculated using both MCM and error propagation methods for $NHV > 200$ BTU/SCF. The insert shows the uncertainties of 70 test cases for PMM measurement using both methods.

The DRE discrepancy between JZ and PMM measurement becomes larger as NHV decreases. The measurement discrepancy is correlated with the uncertainties for both JZ measurement and PMM measurement as shown in Figure 7. The average uncertainty (2σ)

for JZ empirical measurement is $\pm 0.40\%$ for regions of $\text{NHV} > 300 \text{ BTU/SCF}$, which is comparable to the $\pm 0.37\%$ uncertainty calculated from MCM analysis for the PMM method. For regions of $250 < \text{NHV} < 300 \text{ BTU/SCF}$, the average uncertainty (2σ) of DRE% measurement is $\pm 2.72\%$. For regions of $170 < \text{NHV} < 250 \text{ BTU/SCF}$, the average DRE% uncertainty (2σ) is $\pm 10.88\%$. These measurement uncertainties are comparable to the DRE discrepancy between JZ test and PMM measurement in the regions, with the values of 3.63% and 10.59% for regions of $250 < \text{NHV} < 300 \text{ BTU/SCF}$ and $170 < \text{NHV} < 250 \text{ BTU/SCF}$, respectively. The fact that the DRE discrepancy and measurement uncertainties for both methods are comparable shows that this PMM is a reliable method for CE/DRE measurement.

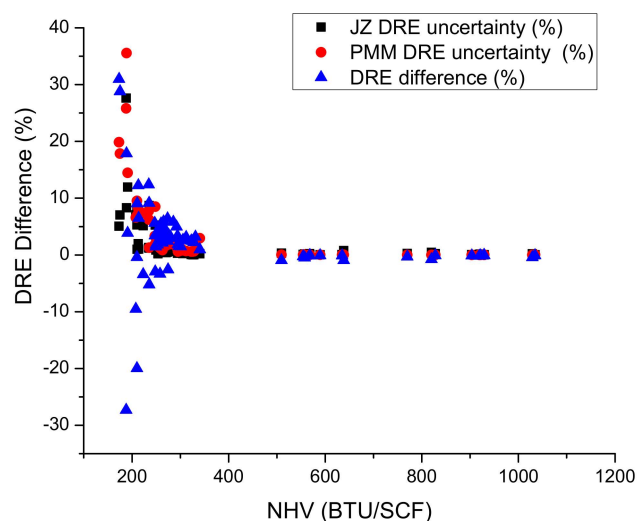


Figure 7. Correlation between the DRE uncertainties of both JZ measurement and PMM measurement to their DRE difference.

The behavior of the increasing measurement uncertainty in the CE/DRE transitional region has also been reported by others in flare studies using the extractive sampling method, for example as shown in the paper by Wormhoudt [21]. This real phenomenon is because of the inhomogeneities in the plumes, which leads to larger variation in sample extraction as well as the high sensitivity of CE/DRE to NHV changes in this region. According to the uncertainty analysis using the error propagation method for the PMM model, a 1% error in NHV measurement would cause 6.79% error in DRE at $\text{NHV} = 200 \text{ BTU/SCF}$, while the corresponding error would be 0.01% for $\text{NHV} = 600 \text{ BTU/SCF}$. For the $\text{NHV} < 300 \text{ BTU/SCF}$ region, errors caused by sample extraction are also a major cause. This error could be dramatically reduced if all of the flare plume gas could be collected and analyzed.

3.3. MW Measurement from Speed of Sound

As mentioned above, a complete flare CE/DRE measurement and monitoring system can be built around ultrasonic flowmeters, since MW and NHV can be derived from sound speed measurement provided by the flowmeters. The method of deriving the vent gas mixture average MW from speed of sound (SOS) was described in the patent by Hammond [14]. The typical error in MW calculation is within 2% for hydrocarbon mixtures. The vent gas MW measured from FTIR and speed of sound method and their difference for all the test points were listed in Table A3. The MW measured from the ultrasonic flowmeter was calibrated in the manufacturing facility before shipping to the John Zink test facility and was installed without further calibration using the field gas. The performance for the JZ test is plotted in Figure 8. As shown in the plot, the linear fit of MW from SOS method and FTIR measurement yield a slope of 0.9926 and slightly negative MW offset of -0.499 g/mol for the MW range. The average error in SOS MW calculation is -2.84% compared to that from FTIR, mainly due to the negative MW offset, which could be further reduced by using a field gas calibration for applications with known gas composition.

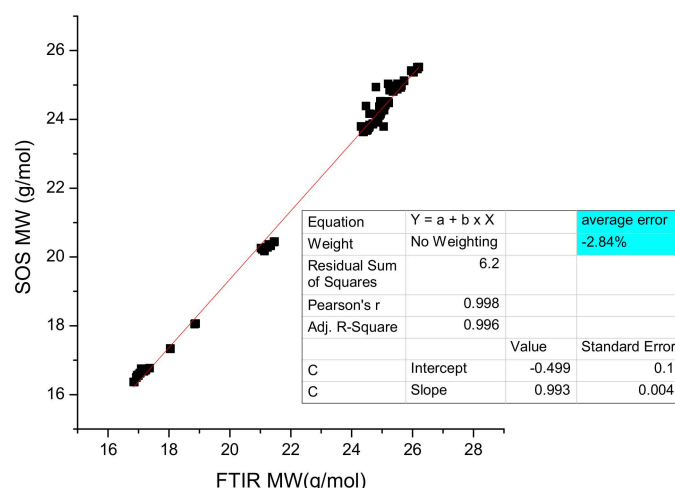


Figure 8. Correlation between the vent gas MW measured by FTIR and by speed of sound method. The fitting results are listed in the table inserted. The black dots are measured MW from sound speed; red line is the fitted MW. Highlighted in the blue box is the average error of MW from SOS.

The NHV of hydrocarbons can be readily calculated from the average MW, as it is proportional to MW. This method of deriving MW/NHV from SOS has also been implemented for active flare control to resolve the gas chromatograph (GC) latency problem, which has a typical response time of 8 to 15 min as demonstrated by Johnson et al. [22]. This feature can provide flare operators with important information to properly operate their flares in terms of controlling NHV in the combustion zone and assist-to-flare gas ratio, especially for flares without online gas/BTU analyzers.

Therefore, the average MW can be derived from flare gas sound speed provided by an ultrasonic flare flowmeter. Subsequently, the NHV of flare gas can be derived from the MW. Both MW and NHV are critical information required for the operation of assisted flares and flare efficiency measurement.

4. Discussion

Accurate measurement of flare emissions, preventing methane slip and evaluating the environmental impact, requires individual flares to be monitored on a near-continuous basis. Using a single value, such as a flare tip designed with a combustion of 98%, regardless of known influence of flare operation conditions and environmental conditions, specifically crosswind, could lead to both under- and over-estimation of flare emissions. Any upcoming carbon tax, such as the US's proposed rules on methane emission [3], the EU Emission Trade System (ETS), and the upcoming new regulations aiming at curbing methane emissions [23], also requires meaningful and accurate emission measurement.

The real-time CE/DRE measurement system will provide accurate emission measurement rather than using a fixed number. The fact that CE/DRE has shown large variations for different flares from recent airborne studies suggests that individual flare CE/DRE monitoring is critical for accurate flare emissions measurement and management [2]. The validation test has also shown large variations in flare efficiency, mainly depending on process conditions, such as flare gas heating value. For NHV < 300 BTU/SCF, flare combustion is unstable and exhibits sensitivity to flowrate and crosswind. Flare efficiency varies in a wide range from 40% to >98%, while the DRE will be >98% and is less sensitive to crosswind and flowrate for NHV > 300 BTU/SCF.

Recently, the development of flare combustion efficiency measurement and monitoring using remote sensing technologies has shown some success in field applications, but flare combustion efficiency measurement and monitoring is still a technological challenge, especially for reliability and accuracy. Even though P-FTIR [10] and hyperspectral imager [12] have demonstrated very high accuracy in flare CE measurement, the success

has been limited mainly due to system complexity, cost, and reliability. The use of PMM models therefore has the potential to close an important knowledge gap and to provide reliable real-time flare CE/DRE measurement for a wide range of operation conditions. In particular, this PMM method has shown an average accuracy of 0.85% for DRE for the NHV > 300 BTU/SCF region where flare is supposed to operate with high efficiency.

This is combined with the ultrasonic flowmeter, where key parameters affecting flare combustion efficiency, such as vent gas flowrate, MW, and NHV, can be derived from the sound speed measurement of ultrasonic flowmeter. The method requires little or no updating to hardware for any existing flare systems to achieve continuous flare combustion efficiency monitoring. For any flare systems with ultrasonic flowmeters, the only hardware update required is an industrial computer loaded with this PMM model, which can communicate with the DCS via Modbus. The minimum overhead and maintenance cost, coupled with the simplicity and reliability of the overall system, make this PMM method a practical and scalable technique for real-time flare efficiency monitoring.

This versatile PMM method can be extended to other flare systems. Based on the same concept, models for assisted flares (steam or air assisted) have also been developed for downstream flare applications. Accurate flare CE measurement or monitoring would not only assist flare operators in optimizing their flare operations, but also provide regulatory agencies with the full picture of methane emissions in corresponding policy making.

5. Conclusions

Flare combustion is such a dynamic process that its efficiency can be affected by operation process as well as environmental conditions, especially crosswind. There are a few ways to measure flare combustion efficiency on a full-scale flare, but it has been a long-standing challenge to monitor flare CE/DRE. Remote sensing techniques, such as DIAL, pFTIR, and hyperspectral imager, are great alternatives to the extractive sampling method for measuring flare CE/DRE. But they have limited success to be scaled up in field applications due to system complexity and high cost.

The new method, which is based on generalizing the factors affecting flare combustion efficiency, has been verified using the extractive sampling method for 70 test points covering various operation conditions with three full-scale flares. The measured CE/DRE has shown large variation from 40% to 99+%, mainly due to flare operation conditions. This test not only filled the gap in upstream flare efficiency measurement data availability, but also validated the PMM-based flare efficiency measurement and monitoring system. It has been verified to provide reliable CE/DRE measurement for flares with no assists. Specifically, for regions where flares are designed to operate with high efficiency (i.e., NHV > 300 BTU/SCF), this PMM method has an average error of 0.83% (absolute) in DRE measurement. The PMM method enables accurate measurement of CE/DRE, which allows accurate reporting of emissions from oil and gas production facilities. For regions where flare is not stable, a larger discrepancy between the empirical test and the new PMM measurement was observed, which correlated to the increasing uncertainties for both methods. With more test data or reliable CFD results available, the parametric model can be further refined to provide more accurate results for conditions even beyond this test.

Coupling this with the method of deriving MW and NHV from the flare gas speed of sound measurements provided by ultrasonic flowmeters, a simplified system built upon ultrasonic flowmeter provides real-time flare CE/DRE measurement and monitoring. The complete system for flare CE/DRE measurement has been employed, and performance has been verified through empirical testing. This simplified flare efficiency measurement system can be readily deployable and scaled up for existing flares with minimum hardware updating.

Author Contributions: Design and execution of the experiments was conducted by the authors (C.T., J.C., A.W., L.S., G.B., P.E., D.N., R.V., J.L. (Jon Lowe) and J.L. (Johan Liekens)). Data processing was led by C.T. The final manuscript was prepared by C.T. All authors have read and agreed to the published version of the manuscript.

Funding: This research was funded by BP and Baker Hughes.

Institutional Review Board Statement: Not applicable.

Informed Consent Statement: Not applicable.

Data Availability Statement: The data presented in this study are available on request from the corresponding author. The data are not publicly available due to privacy.

Acknowledgments: The authors are grateful for the support of colleagues in BP and Baker Hughes in the execution of this project and for the research collaboration that underpins it with special thanks to Jacob Freeke and Jinfeng Zhang. We thank Marco Rocha, Christopher Blake, and Brian Reeves for running the Monte Carlo uncertainty analysis. We would also like to recognize the work of the team at the John Zink facility in Tulsa for the safe management of the tests and provision of the pipe and hydra flare tips. We are also grateful to GBA flare systems for the design, manufacture, and loan of the sonic flare tip.

Conflicts of Interest: Chong Tao, Jon Chow, Lei Sui, Anan Wang, and Gerard Bottino are employees of Baker Hughes. Peter Evans, David Newman, Raj Venuturumilli, Johan Liekens, and Jon Lowe are employees of bp. This research was funded by bp and Baker Hughes. The paper reflects the views of the authors and not those of BP or Baker Hughes.

Appendix A

Table A1. Experiment test conditions.

Test No.	Flare Type	TNG Flowrate (SCFH)	N2 Flowrate SCFH)	NHVvg (BTU/SCF)
1	Utility Flare	1591	0	912
2	Utility Flare	39,267	0	929
3	Utility Flare	25,315	13,461	592
4	Utility Flare	3080	1648	559
5	Utility Flare	1014	550	555
6	Utility Flare	12,661	25,628	305
7	Utility Flare	1559	3103	298
8	Utility Flare	510	1049	283
9	Utility Flare	11,371	27,714	270
10	Utility Flare	1376	3367	258
11	Utility Flare	454	1114	235
12	Utility Flare	10,542	28,402	260
13	Utility Flare	1272	3476	253
14	Utility Flare	8666	30,313	213
15	Utility Flare	1053	3702	227
16	Utility Flare	1563	0	929
17	Utility Flare	1549	3208	283
18	Utility Flare	1563	3145	295
19	Utility Flare	1355	3311	270
20	Utility Flare	10,573	28,281	269
21	Utility Flare	1256	3427	252
22	Utility Flare	1267	3441	248
23	Utility Flare	8559	30,554	220
24	Utility Flare	341	1216	214
25	Sonic	8572	0	928
26	Sonic	347	0	666
27	Sonic	5748	3088	576
28	Sonic	682	371	513
29	Sonic	233	126	471
30	Sonic	2885	5822	299
31	Sonic	339	707	271
32	Sonic	115	243	249
33	Sonic	2528	6152	264
34	Sonic	306	743	251

Table A1. Cont.

Test No.	Flare Type	TNG Flowrate (SCFH)	N2 Flowrate SCFH)	NHVvg (BTU/SCF)
35	Sonic	1220	3004	258
36	Sonic	1131	3074	247
37	Sonic	570	1519	240
38	Sonic	286	770	240
39	Sonic	1921	6821	212
40	Sonic	234	809	201
41	Sonic	902	3161	212
42	Sonic	1483	7231	157
43	Sonic	366	1753	170
44	Sonic	1050	0	932
45	Sonic	5551	3065	572
46	Sonic	1395	2859	291
47	Sonic	1389	2813	293
48	Sonic	1382	2829	296
49	Sonic	114	239	306
50	Sonic	571	1535	249
51	Sonic	562	1531	247
52	Sonic	577	1536	247
53	Sonic	238	815	223
54	Sonic	1496	7170	158
55	Sonic	363	1714	169
56	Hydra	43,543	0	923
57	Hydra	8726	0	904
58	Hydra	1050	0	771
59	Hydra	2098	0	828
60	Hydra	5695	3148	567
61	Hydra	1372	738	553
62	Hydra	2918	5855	294
63	Hydra	717	1419	263
64	Hydra	2528	6186	258
65	Hydra	1221	2970	259
66	Hydra	2341	6363	247
67	Hydra	1134	3028	250
68	Hydra	1937	6782	210
69	Hydra	1744	6969	191
70	Hydra	936	3269	210

Table A2. Flare validation test results.

Test No.	JZ CE (%)	JZ CE Uncertainty (1σ) (%)	JZ DRE (%)	JZ DRE Uncertainty (1σ) (%)	PMM CE (%)	PMM CE Uncertainty (1σ) (%)	PMM DRE (%)	PMM DRE Uncertainty (1σ) (%)	DRE Difference (%)	PMM CE Uncertainty MCM (2σ) (%)	PMM DRE Uncertainty MCM (2σ) (%)
1	99.69%	0.12%	99.84%	0.11%	99.52%	0.01%	100.00%	0.01%	-0.16%	0.001%	0.00%
2	99.92%	0.03%	99.95%	0.02%	99.37%	0.01%	100.00%	0.01%	-0.05%	0.01%	0.00%
3	99.86%	0.05%	99.91%	0.03%	99.26%	0.01%	100.00%	0.01%	-0.09%	0.01%	0.00%
4	99.16%	0.27%	99.52%	0.17%	99.14%	0.02%	100.00%	0.01%	-0.48%	0.02%	0.00%
5	99.63%	0.10%	99.73%	0.09%	99.13%	0.03%	100.00%	0.02%	-0.27%	0.02%	0.00%
6	99.12%	0.58%	99.65%	0.23%	95.49%	0.94%	97.03%	0.79%	2.62%	1.48%	1.25%
7	97.29%	1.46%	98.50%	1.05%	95.36%	0.79%	96.88%	0.66%	1.62%	1.25%	1.06%
8	95.73%	1.96%	96.65%	2.09%	93.85%	2.68%	95.53%	2.27%	1.12%	4.35%	3.75%
9	98.65%	0.49%	99.16%	0.42%	93.04%	1.94%	94.96%	1.64%	4.19%	3.59%	3.08%
10	88.09%	4.69%	91.96%	4.46%	93.42%	1.43%	95.24%	1.21%	-3.28%	2.84%	2.42%
11	86.16%	9.12%	88.64%	8.70%	91.92%	1.52%	93.87%	1.28%	-5.23%	2.61%	2.22%
12	97.38%	1.22%	98.55%	0.95%	90.69%	3.54%	92.97%	3.03%	5.58%	6.74%	5.92%
13	92.47%	2.12%	95.77%	2.18%	91.92%	2.83%	93.96%	2.41%	1.81%	6.03%	5.26%
14	95.19%	1.78%	96.92%	1.98%	80.63%	9.33%	84.26%	8.24%	12.66%	15.38%	14.43%
15	73.99%	5.38%	81.66%	5.17%	86.67%	7.59%	89.44%	6.60%	-7.78%	19.21%	17.97%
16	99.92%	0.03%	99.92%	0.03%	99.53%	0.01%	100.00%	0.01%	-0.08%	0.00%	0.00%
17	98.76%	0.47%	99.30%	0.36%	96.38%	0.82%	97.74%	0.69%	1.55%	1.36%	1.15%
18	98.66%	0.53%	99.26%	0.44%	96.00%	0.70%	97.42%	0.58%	1.84%	1.16%	0.98%

Table A2. Cont.

Test No.	JZ CE (%)	JZ CE Uncertainty (1σ) (%)	JZ DRE (%)	JZ DRE Uncertainty (1σ) (%)	PMM CE (%)	PMM CE Uncertainty (1σ) (%)	PMM DRE (%)	PMM DRE Uncertainty (1σ) (%)	DRE Dif-ference (%)	PMM CE Uncertainty MCM (2σ) (%)	PMM DRE Uncertainty MCM (2σ) (%)
19	97.90%	0.62%	98.86%	0.62%	93.98%	1.56%	95.71%	1.32%	3.15%	3.18%	2.72%
20	99.38%	0.41%	99.73%	0.19%	92.86%	2.38%	94.81%	2.02%	4.92%	5.32%	4.61%
21	93.74%	2.75%	96.39%	2.84%	92.28%	2.51%	94.27%	2.13%	2.13%	5.51%	4.78%
22	96.47%	1.36%	98.06%	1.31%	92.53%	2.19%	94.48%	1.85%	3.58%	4.79%	4.13%
23	97.37%	1.28%	98.98%	0.98%	85.25%	7.76%	88.29%	6.76%	10.69%	19.35%	18.15%
24	96.81%	1.49%	98.29%	1.03%	89.46%	8.49%	91.72%	7.36%	6.56%	20.15%	18.73%
25	98.82%	0.56%	99.57%	0.18%	99.35%	0.01%	100.00%	0.01%	−0.43%	0.01%	0.00%
26	98.25%	1.39%	99.20%	0.46%	99.51%	0.01%	100.00%	0.01%	−0.80%	0.00%	0.00%
27	97.70%	1.61%	99.04%	0.76%	99.08%	0.03%	100.00%	0.03%	−0.96%	0.02%	0.00%
28	99.64%	0.11%	99.74%	0.09%	98.95%	0.03%	99.84%	0.03%	−0.10%	0.02%	0.00%
29	98.41%	0.31%	98.80%	0.30%	98.97%	0.06%	99.73%	0.05%	−0.93%	0.02%	0.00%
30	98.91%	0.32%	99.33%	0.31%	94.48%	1.09%	96.16%	0.92%	3.16%	1.51%	1.28%
31	95.70%	0.96%	97.11%	0.95%	94.79%	1.44%	96.27%	1.21%	0.84%	1.67%	1.41%
32	91.81%	1.30%	91.71%	2.41%	92.27%	3.84%	93.91%	3.23%	−2.20%	1.93%	1.64%
33	98.48%	0.67%	99.02%	0.58%	91.57%	1.90%	93.69%	1.61%	5.33%	3.24%	2.78%
34	97.07%	0.90%	97.84%	0.88%	93.64%	2.25%	95.28%	1.89%	2.55%	3.21%	2.74%
35	97.69%	0.59%	98.63%	0.62%	90.86%	2.33%	93.06%	1.98%	5.57%	3.98%	3.44%
36	96.67%	0.56%	96.78%	1.21%	88.38%	3.94%	90.93%	3.38%	5.85%	7.11%	6.28%
37	97.48%	1.11%	98.28%	1.01%	91.42%	2.48%	93.47%	2.10%	4.81%	4.92%	4.25%
38	96.24%	2.09%	97.04%	1.92%	93.06%	3.21%	94.78%	2.72%	2.26%	5.25%	4.54%
39	96.50%	1.24%	98.16%	1.32%	82.50%	8.79%	85.85%	7.72%	12.31%	16.43%	15.38%
40	84.27%	2.64%	85.21%	5.14%	85.73%	8.48%	88.40%	7.33%	−3.19%	16.64%	15.25%
41	96.37%	1.04%	97.65%	1.19%	85.68%	7.16%	88.57%	6.23%	9.08%	17.24%	16.00%
42	89.30%	5.31%	93.53%	5.06%	56.59%	21.49%	62.32%	19.88%	31.21%	16.47%	16.60%
43	81.50%	2.74%	82.30%	8.31%	59.30%	50.01%	64.40%	50.00%	17.91%	20.57%	21.00%
44	99.90%	0.03%	99.91%	0.03%	99.53%	0.01%	100.00%	0.01%	−0.09%	0.00%	0.00%
45	99.84%	0.06%	99.88%	0.05%	99.25%	0.02%	100.00%	0.01%	−0.12%	0.01%	0.00%
46	99.69%	0.09%	99.86%	0.06%	96.00%	0.73%	97.42%	0.61%	2.44%	1.20%	1.01%
47	99.73%	0.07%	99.89%	0.05%	95.84%	0.70%	97.28%	0.58%	2.61%	1.14%	0.96%
48	99.83%	0.06%	99.88%	0.05%	96.22%	0.75%	97.60%	0.63%	2.28%	1.21%	1.02%
49	99.26%	0.09%	99.36%	0.21%	97.59%	3.51%	98.44%	2.95%	0.91%	2.14%	1.81%
50	96.72%	0.69%	98.37%	0.69%	93.04%	2.57%	94.86%	2.18%	3.52%	5.37%	4.64%
51	94.82%	3.68%	96.86%	2.78%	92.64%	2.90%	94.52%	2.46%	2.35%	6.03%	5.23%
52	97.76%	0.47%	98.77%	0.48%	93.34%	2.29%	95.11%	1.94%	3.66%	4.69%	4.04%
53	86.89%	4.89%	89.60%	5.27%	90.68%	9.80%	92.71%	8.51%	−3.11%	19.72%	18.34%
54	86.73%	7.06%	93.37%	7.03%	57.83%	19.48%	63.48%	17.86%	29.89%	17.55%	17.57%
55	49.63%	17.38%	45.97%	27.62%	69.20%	27.74%	73.67%	25.82%	−27.70%	19.33%	19.57%
56	99.79%	0.14%	99.88%	0.13%	99.21%	0.01%	100.00%	0.01%	−0.12%	0.03%	0.00%
57	99.79%	0.06%	99.88%	0.06%	99.38%	0.01%	100.00%	0.01%	−0.12%	0.02%	0.00%
58	99.38%	0.32%	99.68%	0.25%	99.44%	0.01%	100.00%	0.01%	−0.32%	0.01%	0.00%
59	99.83%	0.27%	99.91%	0.22%	99.47%	0.01%	100.00%	0.01%	−0.09%	0.01%	0.00%
60	99.70%	0.10%	99.87%	0.07%	99.10%	0.03%	100.00%	0.02%	−0.13%	0.02%	0.00%
61	99.86%	0.23%	99.87%	0.23%	99.32%	0.02%	100.00%	0.02%	−0.13%	0.02%	0.00%
62	97.98%	0.41%	98.92%	0.30%	93.91%	1.23%	95.68%	1.04%	3.23%	1.64%	1.39%
63	94.39%	2.38%	96.02%	2.05%	92.27%	1.03%	94.22%	0.87%	1.80%	1.35%	1.14%
64	96.19%	1.29%	97.87%	1.04%	91.28%	2.31%	93.44%	1.96%	4.43%	3.76%	3.24%
65	95.48%	1.19%	97.11%	0.98%	91.68%	2.05%	93.75%	1.74%	3.36%	3.56%	3.07%
66	93.99%	1.85%	96.46%	1.38%	87.63%	3.88%	90.32%	3.33%	6.14%	6.76%	5.95%
67	92.59%	0.76%	95.29%	0.85%	91.23%	2.50%	93.36%	2.12%	1.92%	5.09%	4.41%
68	57.51%	6.03%	62.56%	8.58%	79.06%	10.70%	82.83%	9.52%	−20.27%	14.09%	13.25%
69	74.09%	11.00%	80.82%	11.95%	72.32%	15.90%	76.82%	14.47%	4.00%	13.99%	13.58%
70	81.59%	6.00%	86.47%	5.29%	84.20%	7.92%	87.29%	6.92%	−0.82%	17.10%	15.95%

Table A3. Vent gas MW measured from FTIR and speed of sound (SOS).

Test No.	MW from FTIR (g/mol)	SOS MW (g/mol)	Delta MW (g/mol)	Error (%)
1	17.18	16.76	−0.43	−2.49
2	17.05	16.62	−0.43	−2.52
3	21.06	20.24	−0.81	−3.87
4	21.33	20.33	−1	−4.67
5	21.46	20.44	−1.02	−4.74
6	24.43	23.76	−0.67	−2.73
7	24.51	23.71	−0.8	−3.25
8	24.66	23.85	−0.81	−3.27
9	24.88	24.2	−0.68	−2.75
10	24.8	24.15	−0.65	−2.62
11	24.95	24.52	−0.42	−1.7
12	25.21	24.48	−0.73	−2.9

Table A3. Cont.

Test No.	MW from FTIR (g/mol)	SOS MW (g/mol)	Delta MW (g/mol)	Error (%)
13	24.91	24.37	−0.55	−2.2
14	25.01	24.43	−0.58	−2.33
15	25.46	24.97	−0.49	−1.92
16	25.32	24.94	−0.38	−1.51
17	25.58	24.97	−0.61	−2.39
18	25.61	24.99	−0.63	−2.44
19	16.96	16.55	−0.41	−2.43
20	24.65	23.79	−0.85	−3.47
21	24.53	23.74	−0.79	−3.21
22	24.81	24.17	−0.64	−2.59
23	24.83	24.39	−0.45	−1.8
24	25.02	24.41	−0.6	−2.42
25	25.08	24.42	−0.66	−2.62
26	25.4	25.03	−0.37	−1.46
27	25.48	24.91	−0.57	−2.23
28	16.85	16.37	−0.49	−2.89
29	21.13	20.18	−0.95	−4.51
30	24.58	23.8	−0.78	−3.18
31	24.56	23.77	−0.8	−3.25
32	24.98	24.23	−0.74	−2.98
33	25.05	24.28	−0.77	−3.07
34	24.94	24.18	−0.76	−3.04
35	25.06	24.4	−0.66	−2.64
36	25.07	24.4	−0.67	−2.67
37	25.17	24.52	−0.66	−2.6
38	25.19	24.52	−0.67	−2.65
39	25.18	24.49	−0.69	−2.75
40	25.55	25	−0.55	−2.16
41	25.63	24.99	−0.65	−2.53
42	25.51	24.93	−0.58	−2.27
43	26.19	25.52	−0.67	−2.56
44	25.96	25.42	−0.55	−2.11
45	16.98	16.57	−0.42	−2.45
46	21.28	20.36	−0.92	−4.31
47	24.59	23.8	−0.79	−3.21
48	24.56	23.77	−0.79	−3.22
49	24.53	23.78	−0.76	−3.09
50	24.41	23.65	−0.76	−3.11
51	25.06	24.45	−0.62	−2.47
52	25.08	24.48	−0.61	−2.42
53	25.1	24.42	−0.68	−2.71
54	25.36	24.81	−0.55	−2.18
55	26.16	25.47	−0.69	−2.64
56	26.03	25.37	−0.66	−2.52
57	16.95	16.51	−0.44	−2.6
58	17.22	16.71	−0.52	−3
59	18.86	18.06	−0.8	−4.26
60	18.05	17.34	−0.71	−3.94
61	21.29	20.33	−0.96	−4.52
62	24.51	23.69	−0.82	−3.35
63	24.87	23.92	−0.95	−3.83
64	24.94	24.15	−0.79	−3.16
65	24.91	24.11	−0.8	−3.2
66	25.07	24.39	−0.68	−2.71
67	25.02	24.33	−0.69	−2.76
68	25.49	24.88	−0.61	−2.4
69	25.72	25.12	−0.6	−2.33
70	25.49	24.88	−0.61	−2.38

References

1. Available online: <https://www.worldbank.org/en/programs/gasflaringreduction/publication/2023-global-gas-flaring-tracker-report> (accessed on 20 November 2023).
2. Plant, G.; Kort, E.; Brandt, A.; Chen, Y.; Negron, A.; Schwietzke, S.; Smith, M.; Zavala-Ariaiza, D. Inefficient and unlit natural gas flares both emit large quantities of methane. *Science* **2022**, *377*, 1566–1571. [[CrossRef](#)] [[PubMed](#)]
3. US Environmental Protection Agency. *Greenhouse Gas Reporting Rule: Revisions and Confidentiality Determinations for Petroleum and Natural Gas System 2023*; American Gas Association: Washington, DC, USA, 2023.
4. McDaniel, M.; Tichenor, B.A. Flare Efficiency Study. 1983. Available online: https://gaftp.epa.gov/ap42/ch13/s05/reference/ref_01c13s05_jan1995.pdf (accessed on 22 November 2023).
5. Allen, D.; Torres, V. TCEQ 2010 Flare Study Final Report. 2011. Available online: https://downloads.regulations.gov/EPA-HQ-OAR-2012-0133-0047/attachment_32.pdf (accessed on 22 November 2023).
6. Johnson, M.; Kostiuk, L. A parametric model for the efficiency of a flare in crosswind. *Proc. Comb. Inst.* **2002**, *29*, 1943–1950. [[CrossRef](#)]
7. Edgar, T.; Castineira, D. Computational fluid dynamics for simulation of wind-tunnel experiments on flare combustion systems. *Energy Fuels* **2008**, *22*, 1698–1706. [[CrossRef](#)]
8. Singh, K.; Gangadharan, P.; Dabade, T.; Shinde, V.; Chen, D.; Lou, H.; Richmond, P.; Li, X. Parametric study of ethylene flare operations using numerical simulation. *Eng. App. Comp. Flu. Mech.* **2014**, *8*, 211–228. [[CrossRef](#)]
9. Germanou, L.; Newman, D.; Black, S.; Laing, M. Metering and emission analysis of flare and vent metering systems using Computational Fluid Dynamics. In Proceedings of the Global Flow Measurement Workshop, Aberdeen, UK, 25–27 October 2022.
10. Performance Test of a Steam-Assisted Elevated Flare with Passive FTIR Final Report, Prepared by Clean Air Engineering Inc.; Project No: 10810 for Marathon Petroleum Company, LLC Texas Refining Division. 2010. Available online: https://downloads.regulations.gov/EPA-HQ-OAR-2012-0133-0047/attachment_17.pdf (accessed on 22 November 2023).
11. Chambers, A.K.; Wootton, T.; Moncrieff, J.; McCready, P. *Combustion Efficiency of Full Scale Flares Measured Using DIAL Technology*; American Flame Research Committee: Lakewood Ranch, FL, USA, 2003. Available online: <https://collections.lib.utah.edu/ark:/87278/s6dn9777> (accessed on 22 November 2023).
12. Zeng, Y.; Morris, J.; Dombrowski, M. Validation of a new method for measuring and continuously monitoring the efficiency of industrial flares. *J. Air Waste Mgmt. Assoc.* **2016**, *66*, 76–86. [[CrossRef](#)] [[PubMed](#)]
13. Tao, C.; Weling, A.; Sui, L.; Kowal, A.; Muller, M. Emission Monitoring of Flare Systems. U.S. Patent 2021/0372864A1, 12 February 2021.
14. Hammond, R. Ultrasonic Measurement System with Molecular Weight Determination. U.S. Patent 6,216,091B1, 10 April 2009.
15. Tao, C.; Johnson, D.; Weling, A.; Kowal, A.; Huang, Y. Online Analyzers for Flare Gas Processing. U.S. Patent 2022/0107289A1, 7 April 2022.
16. Evans, P.; Tao, C.; Newman, D.; Chow, J.; Venuturumilli, R.; Wang, A.; Lowe, J.; Liekens, J.; Sui, L.; Bottino, G. Full-size experimental measurement of combustion and destruction efficiency in unassisted flares and the implications for control of methane emissions from oil and gas production. *Atmosphere* **2024**, *15*, 333. [[CrossRef](#)]
17. EPA Method 19—Determination of Sulfur Dioxide Removal Efficiency and Particulate Matter, Sulfur Dioxide, and Nitrogen Oxide Emission Rates. Available online: <https://www.epa.gov/emc/method-19-sulfur-dioxide-removal-and-particulate-sulfur-dioxide-and-nitrogen-oxides-electric> (accessed on 9 March 2024).
18. *ISO/IEC Guide 98-3:2008*; Evaluation of Measurement Data—Guide to the Expression of Uncertainty in Measurement. ISO: Rome, Italy, 2008.
19. US Environmental Protection Agency. Petroleum Refinery Sector Risk and Technology Review and New Source Performance Standards. 2014. Available online: <https://www.govinfo.gov/content/pkg/FR-2014-06-30/pdf/2014-12167.pdf> (accessed on 22 November 2023).
20. *ISO/IEC GUIDE 98-3/Suppl.1*; Uncertainty of Measurement Part 3: Guide to the Expression of Uncertainty in Measurement (GUM:1995)—Supplement 1: Propagation of Distributions Using a Monte Carlo Method. ISO: Rome, Italy, 2008.
21. Wormhoudt, J.; Herndon, S.; Franklin, J.; Wood, E.; Knighton, B.; Evans, S.; Laush, C.; Sloss, M.; Spellicy, R. Comparison of remote sensing and extractive sampling measurements of flare combustion efficiency. *IEC Res.* **2012**, *51*, 12621–12629. [[CrossRef](#)]
22. Johnson, D.; Tao, C.; Brooks, J.; Pfenniger, R.; Sui, L. Integrated Flare Combustion Control. U.S. Patent US2021/0071865A1, 11 March 2021.
23. EU Passed Law to Curb Methane Emission. Available online: https://ec.europa.eu/commission/presscorner/detail/en/ip_23_5776 (accessed on 9 March 2024).

Disclaimer/Publisher’s Note: The statements, opinions and data contained in all publications are solely those of the individual author(s) and contributor(s) and not of MDPI and/or the editor(s). MDPI and/or the editor(s) disclaim responsibility for any injury to people or property resulting from any ideas, methods, instructions or products referred to in the content.